A Unified View of the Origin and Morphology of the Turbulent Boundary Layer Structure

K.R. SREENIVASAN

Mason Laboratory, Yale University
New Haven, CT 06520

Summary

On the basis of instability and vortex interactions in an idealized physical model, an attempt is made to deduce in a self-contained and rational way the structure of the turbulent boundary layer. It is shown that the model provides a rough but self-consistent description of several known aspects of the structure.The key concept is that of a 'critical layer' in the flow. It is believed that this description will shed some light on possible control schemes for the turbulent boundary layer.

1. Introduction

Among the prototypical turbulent flows repeatedly studied over the years, the turbulent boundary layer (TBL) is clearly the least understood in terms of its structure. One of the primary difficulties is that there are at least two distinct scales in the flow which are disparate at high Reynolds numbers, and the interaction of phenomena dominated by one scale with those dominated by the other is generally ill-understood.

It should thus come as no surprise that the experimental work has identified a multiplicity of structural elements. For example, some evidence has been put forth (Townsend 1966; Kovasznay, Kibens & Blackwelder 1970) to suggest that the boundary layer is domimated by the so-called large eddies of size comparable to the entire thickness of the boundary layer. On the other hand, more recent evidence (Head & Bandyopadhyay 1981) suggests that the very existence of these structures is in doubt, and that the large eddy apparent in flow visualization studies is only the slow overturning motion of a collection of smaller scale eddies of the hairpin type, each of which is inclined, over a major part of the thickness, at around 45^{o} to the plane of the flat plate. In fact, hypotheses have been made (Perry & Chong 1982) that the essential structure of the flow is a hierarchy of hairpin eddies. Other structural elements such as the 'typical' eddies (Falco 1977), double roller-type eddies (Townsend 1956, Kim & Moin 1986, Nagib & Guezennec 1986), transverse vortices (Praturi & Brodkey 1978), have also been identified.

H.W. Liepmann, R. Narasimha (Eds.)
Turbulence Management and Relaminarisation

In the inner layer where the characteristic scale is governed by the wall shear stress and viscosity, the evidence appears incontrovertible - at least at low Reynolds numbers - that an important feature is the streaky structure (Kline et al. 1967). The sequence of quasiperiodic events comprising of the formation of these streaks, and the lift-up, oscillation and breakdown of some of them, together designated as the bursting process (Kline 1978), is believed to be responsible for the significant fraction of the turbulent energy production (Kim, Kline & Reynolds 1971). Research has also revealed the existence of other structures, for example, pockets (Falco 1987).

It is clear that the TBL structure is many-faceted and complex. Even if we concede that some of these structural elements are not independent - that is, they emphasize different aspects of the same basic form - we are still left with a number of them, and the puzzle is to decide which of them are dynamically significant, and how they arise and interact. If, for the sake of the argument, we assume that the large structure is indeed the dominant and driving mechanism, the question arises as to how it originates and maintains itself. Clearly, we can rule out laminar-turbulent transition as the source. It is also not hard to argue that the bursting process is unlikely to accomplish this, merely based on the fact that its scales and the large eddy are quite disparate at high Reynolds numbers; to our knowledge, no one has observed the required hierarchical amalgamation of scales to make the point of view viable. Alternatively hypothesizing that bursting is the dominant aspect shifts our concern to its origin and sustained maintenance, and difficulties still remain. If we argue (e.g., Blackwelder 1978) that bursting arises purely from local instabilities in the inner region (say, $y^+ < 30$), it is tantamount to saying, at high Reynolds numbers, that an extremely small fraction of the entire thickness (0.001 at a boundary layer Reynolds number of 10^6) drives the rest of the flow having no active role - a sentiment clearly open to doubt. If we propose instead that bursting is driven by the outer structure (Rao, Narasimha & Badri Narayanan 1971), the nature of the inner/outer interaction has to be understood, and we are back to asking how the outer structure which drives the phenomenon came into being in the first place.

We may conclude that, in spite of some very important work on the topic, no self-contained and complete picture of the structure exists today. It is our belief that, on the shoulders of the past work, such a picture can now be constructed, in a way that explains to a first approximation at least the important structural features of the flow. It is to an assessment of this statement that the paper is devoted. The work is clearly unfinished and has a number of holes, and yet these notes seemed useful if only because they will provide a target for useful criticism.

2. The overall strategy

To set the stage, it is helpful to examine the origin of the dominant structure in the simpler case of a two-dimensional mixing layer between two streams of unequal speeds. For convenience, we shall think first of a counter-current mixing layer, that is, the one in which the two velocities are equal in magnitude and opposite in sign. This allows us to forget the effect of spatial variation of the flow scales momentarily, but we shall return to it soon. Let us consider the laminar case. It is well known that the vortex sheet, formed when the two streams come in contact with each other, is unstable to small two-dimensional perturbations (the Kelvin-Helmholtz instability), and the saturation state of this instability corresponds to the roller-type vortical structure. Vortex sheets of infinitesimal thickness are unstable to perturbations of all wavelengths, but in practice the finite thickness due to viscous diffusion enforces an upper cut-off on the unstable wavenumbers. This results in a most amplified instability wavelength (figure 1), and the expectation that this corresponds to the observed one is then quite natural. If the two-dimensional roller-type structures were to survive, we should show in addition that they are stable to three-dimensional perturbations. Ideally, one should consider the case of arbitrarily large three-dimensional perturbations, but experience in a number of similar circumstances (Gaster, Kit & Wygnanski 1985, Wygnanski, Champagne & Marasli 1986, Wygnanski 1987) suggests that the use of the linear theory may be adequate. This statement calls for a thorough assessment, and some brief remarks are made in section 7, but, for now, we shall take this as an empirical fact.

To show the relation of this picture to the large structure in the turbulent mixing layer, we continue the same descriptive reasoning while clearly recognizing its limitations. If our interest is in the primary large structure, it is our assertion that local or small scale instabilities will not have much influence on the origin of the large structure. This means that, for present purposes, the flow need only be observed and described on scales that coarse-grain the small scale details. Thus viewed, the turbulent mixing layer appears as a vortex sheet much as in the laminar case - although more fattened obviously. This yields roller-type structures whose wavelength we can predict as before. The required three-dimensional stability analysis in this case, carried out by Robinson & Saffman (1982), shows that three dimensional instabilities grow much more slowly, implying that the two-dimensional structures are the most likely ones to be observed. This is qualitatively consistent with observations in turbulent mixing layers.

The task of providing quantitative assessment is rendered difficult because (to our knowledge) there exists no experimental work in constant density counter-current shear flows. There do exist, however, some in slightly stratified environment (Thorpe 1971, 1973; Ramshankar 1986), and an abundance of the spatially

developing type. A quick look at the former class shows that the most amplified wavelength is close to the one observed; more work is needed, however. Quantitative comparisons in spatially developing flows are complicated by the length scale variation with the streamwise direction x. The difficulty is that the observed wavelength at any x is a consequence of the growth from some upstream distance, and it is not clear what length scale one should use to normalize the observed wavelength. If one uses the local length scale (say, the local momentum thickness) the observed dimensionless wavelength of the large structure does not correspond to the largest amplification, but instead to zero amplification. One possible interpretation is that the instability corresponds to the maximum amplification at the point of its onset, but slides down the curve to the right (see figure 1) due to the increasing length scale as it propagates downstream, until the instability saturates (and the structures become observable) at the wavelength of neutral growth. One may conceive of interactions between large structures as the next important step in dynamical evolution.

In sum, the picture is that, insofar as we are interested in the large structure, an appropriate idealization of the mixing layer is a vortex sheet of finite thickness in which the entire mean flow vorticity is being concentrated. It is the end result of its instability to two and three dimensional perturbations that will determine the origin and sustenance of the large structure in the flow. For practical purposes, linear theory seems adequate.The picture appears correct for temporally developing mixing layers, but is qualitatively reasonable for the spatially developing ones also.

These same issues concerning the large structure in other shear flows can now be sought in similar terms by a straightforward procedure. For example, in the case of a two-dimensional wake, we may think of the instability of two vortex sheets of opposite sign as giving the clue to the dominant structure of the wake. We have examined this idea in somewhat of a detail, and roughly satisfied ourselves that the idea is sound there, but this is no place to discuss it. Similar suggestions for other free shear flows are more or less obvious.

It is worth emphasizing that in 'concentrating' all the mean flow vorticity in one or more fat 'sheets', we are no longer concerned about the details of the mean velocity distribution; the implication is that the large-scale instabilities of the two are the same. It follows that one of the *a priori* requirements for the reasonableness of this approach is that the mean velocity distribution itself be unstable. This requirement is obviously satisfied for all free shear flows with inflexion points, but the situation is marginal for the TBL, and certainly different for the channel flow whose mean velocity profile is stable to linear perturbations (Reynolds & Tiederman 1967). The justification for proceeding further in wall-bounded shear flows is merely that the perturbation environment is in general not linear, and that we shall not need to invoke small amplitude perturbations in the primary instability stage.

Now, the inviscid model for the TBL, which obviously reduces to a vortex sheet with a corresponding image, can be expected to be inadequate: unlike the case of the unbounded shear flows where viscosity has no direct influence, a subtle role for it ought to be expected on the basis of previous experience in the transitional case. Even if we succeed in identifying the proper role for viscosity, the vortex sheet is being constantly buffeted around by the small scale stuff generated by the bursting process near the wall, and the details of instability can be quite murky. Finally, it is not *a priori* obvious how far from the wall the vortex sheet must be located. This will clearly play a crucial role in determining the instability of the vortex sheet configuration. The resulting structures can be expected to have a characteristic size of the order of the boundary layer thickness δ itself if we locate the vortex sheet far away from the wall, y/δ fixed around (but less than) unity. This position for the vortex sheet makes little sense, however, because the majority of the TBL vorticity is contained near the wall. On the other hand, putting the vortex sheet in the wall region, yU_*/ν fixed in the inner layer (U_* and ν being the friction velocity and viscosity coefficient respectively), makes the concept of a reasonably well-defined vortex sheet invalid, and the whole idea has to be abandoned. The present view resolving this issue is that something like a 'critical layer' exists in the TBL, and it is precisely here that the vortex sheet must be located. In the following section, we shall argue that this 'critical layer' is similar to the transitional critical layer, and determine its location. (Through out this text, 'critical layer' means the analogy we imply in TBL with the transitional critical layer.)

3. The 'critical layer'

We now make a digression whose relevance will be clear presently. Figure 2a shows the distribution of the Reynolds shear stress in a transitional boundary layer, computed by us from Jordinson's (1970) numerically obtained eigenfunction and eigenvalue data for the unstable Tollmien-Schlichting (T-S) waves. The point of interest here is that the peak in the Reynolds stress coincides with the critical layer. This same remark holds also for the transitional channel flow (figure 2b). We shall now invert this simple finding and stretch its implications significantly by saying that the location of the peak Reynolds shear stress in the TBL is something like a 'critical layer' for the flow. We shall presently determine where in the TBL the Reynolds shear stress peaks, and, to justify the concept of the 'critical layer', show how it shares some of the same properties of the transitional critical layer.

In figure 3a, we have collected all experimental data (including pipe and channel flows) that could be found on the distance y_p from the wall to the location of the peak Reynolds shear stress. The characteristic Reynolds number $R_* = U_*\delta/\nu$ appears naturally as the length scale ratio in the problem. A good fit to the data is given by

$$y_p^+ = y_p U_*/\nu = 2R_*^{0.5}. \qquad (1)$$

Since accurate measurement of the Reynolds stress near the wall is beset with several problems including the probe size, it would be valuable, in view of the importance of (1) in this work, to have some corroborative evidence for the variation seen in figure 3a. In fully developed channel and pipe flows, the Reynolds shear stress distribution is related exactly to the mean velocity distribution U(y) by

$$-\overline{uv} = \nu(dU/dy) + U_*^2(1 - y/a), \qquad (2)$$

where y is the distance normal to the plate and a is the half-channel height or the pipe radius.The mean velocity measurements at distances of interest to us are generally beyond reproach, and so we should be able to obtain the Reynolds shear stress distribution, and thus y_p^+, from the mean velocity data. Figure 3b shows the results in a number of experiments in fully developed pipe and channel flows. Equation (1) describes the variation satisfactorily. It is of interest to note that the lowermost two data points in figure 3b, corresponding respectively to the transitional boundary layer and channel flows of figure 2, obey (1) approximately; this provides some confidence in the present view that the 'critical layer' in the TBL can be thought of as a conceptual extension of the transitional critical layer.

Note 1: Except for the right-most point at R_* of 60000 from Nikuradse's highest Reynolds number experiment, the data in figure 3b do not assume anything but a fully developed state. In the exceptional case, the mean velocity data of Nikuradse did not extend sufficiently close to the wall to include the peak stress location, and was obtained by us by a standard extrapolation to the wall of the mean velocity data before using (2). Although we have enough material to justify (1) without this data point, it was thought that the exercise was worthwhile because of the large Reynolds number of this flow.

Note 2: We may note, without giving proof, that the peak in u' varies only as a weak power of Reynolds number ($R_*^{0.17}$) or perhaps logarithmically. The v' peak is an even stronger function of the Reynolds number than uv. There is considerable scatter in the v' data (much more than for $\overline{uv}$, surprisingly), but the data are roughly consistent with a 0.8 power law. Another possible fit is a constant up to an R_* of 400, and a unit power of R_* beyond. The situation regarding w' (the spanwise component) is quite uncertain.

Two remarks, although obvious from figures 3a and b, are worth making. Firstly,

since the peak in the Reynolds shear stress occurs at increasingly larger y^+ from the wall, we conclude that the part of the dynamics contributing to the Reynolds shear stress does not primarily reside at constant y^+. We shall return to this important point in section 7. Further, the fact that the peak Reynolds stress follows (1) in the TBL as well as pipe and channel flows is here interpreted to mean that the Reynolds shear stress producing motion is similar in all three cases. Secondly, although the peak in the Reynolds shear stress moves outward in terms of wall units, it moves inward in terms of the outer units - in fact, according to the inverse half power of R_*.

It is well known that the flow speed in the transitional critical layer is a constant fraction of the free stream velocity, and it is useful to see if this is true for our 'critical layer' also. Figure 4 shows that, independent of R_*, the speed at the 'critical layer' is a constant of approximately 0.65 U_∞, lending credence to our claim. Other indications justifying the analogy are mentioned in the Appendix.

One observation, although not too directly related, may be useful. For sufficiently high Reynolds numbers, say $R^* > 1000$, the 'critical layer' lies within the logarithmic region of the TBL. We thus have:

$$0.65U_\infty/U_* = A \log y_p^+ + B.$$

Using (1) on the right hand side, we get the result that

$$U_\infty/U_* = 4.3 \log R_* + 8.5, \qquad (3)$$

where we have chosen the usual values of 5.5 for both constants A and B in the log-law. Equation (3) is similar in form to the so-called skin-friction law for the TBL (e.g., Monin & Yaglom, 1971, p 296). The constants in (3) are somewhat different from the usually quoted values of 5.5 and 7.4, but, over a range of R_*, (3) is in substantial agreement with the usual skin friction law. A more detailed assessment should await another occasion.

The picture then is simply the following. The boundary layer is modelled by a fat vortex 'sheet' located at a distance given by (1). To determine the dominant structure of the flow, it is necessary to examine its stability. This is done in the next two sections.

4. The two-dimensional instability of the wall-bounded vortex sheet

According to (1) and our previous discussion, the vortex sheet must be located at $y_p = h = 2(\delta\nu/U_*)^{0.5}$. As this sheet becomes unstable to perturbations, the first task must be to determine the streamwise wavelength of the rolled-up structures (figure 5). Again,

we make the analogy to the transitional case. We propose a heuristic argument to predict the wavelength of the T-S waves, and show that it is in general accordance with observations. We then use the same arguments to determine the wavelength of roll-up in the case of the TBL model.

In the transitional boundary layer, one may imagine a vorticity perturbation imposed on the vortex sheet in the critical layer. There is a corresponding perturbation at the wall, which will both diffuse outwards and convect downstream. If the arrival at the critical layer of the wall perturbation occurs such that it reinforces the vorticity perturbation in the critical layer, the latter will get amplified. If the wall perturbation arrives at the critical layer out of phase with the prevailing perturbation there, the latter will decay and no sustained disturbances are possible. Thus, the criterion for a sustained growth of the vorticity perturbation is that its wavelength be compatible with the phase relationship mentioned above. If $\lambda_{T\text{-}S}$ is the wavelength of a growing T-S wave, and U_c is the phase velocity at the critical layer located distance δ_c from the wall, the condition for reinforcement is

$$\sqrt{\frac{\nu\lambda_{T\text{-}S}}{(1/2)U_c}} = \delta_c$$

where it is assumed that the convection velocity for the wall vorticity perturbation is $0.5U_c$. This relation can be rewritten as

$$\lambda_{T\text{-}S}/\delta = R_\delta/160, \qquad (4)$$

by noting that $\delta_c = 0.19\delta$, and $U_c = 0.35\ U_\infty$. Here, $R_\delta = U_\infty\delta/\nu$. For typical R_δ in the unstable range, we have

$$\lambda_{T\text{-}S}/\delta = O(10),$$

a result close to observation in transitional situations. The usefulness of this argument is that it provides a simple explanation for why the 'aspect ratio' $\lambda_{T\text{-}S}/\delta$ for the T-S waves is of the order 10, while a similar aspect ratio in free shear flows (for example, the mixing layer, and the Karman vortex street) is of the order unity. This also explains why vortex pairing is unlikely in the TBL (secondary instabilities being likely to take over).

Extending this argument to the 'critical layer' in the TBL is conceptually straightforward, but the details need some discussion. This is best done with reference to figure 6. Near the wall in the viscous sublayer (say, $y^+ < 5$), diffusion of the wall vorticity occurs essentially by viscosity, but the major part of the diffusion occurs largely by turbulence. The turbulence intensity profile q'/U_∞ is plotted in figure 6;

$q'^2 = \overline{u'_i\, u'_i}$. (For a self-contained picture of the TBL, we have to say how this turbulence is created, and to this we shall return in section 6. For now, we shall presume that it exists and diffuses the wall vorticity perturbations over the major part of the 'critical layer' height.) If vorticity diffusion by turbulence can be represented by an eddy viscosity ν_e, the above reasoning suggests that

$$\lambda_x/\delta = 1.3\,(\nu/\nu_e)\,(U_\infty/U*). \qquad (5)$$

Although the concept of eddy viscosity as a general rule is not useful in shear layers (for example, Sreenivasan, Tavoularis & Corrsin 1982), its use for mimicking the diffusion effects of small scale turbulence is not too unreasonable. In any case, it is invoked here merely for convenience of completeness, and we shall show that its precise value is immaterial for most of what follows in the next section.

5. The hairpin structure

At this stage, then, we know the distance from the wall of the vortex 'sheet' (equation (1)), and have estimated the streamwise wavelength λ_x of the roll-up structure resulting from the primary instability (equation (5)). Numerical estimates based on (5) will be given later, but it is useful to note that the ratio λ_x/δ is generally of the order 5 over a significant range of Reynolds number.

If this structure is the one to be observed, it must be shown to be stable to three dimensional perturbations. As suggested earlier, we shall be content with inviscid and linear theory. (An effect of viscosity appears in equation 5, and will reappear in a stronger form in section 6. For fast growing modes, which the three-dimensional perturbations actually are, it is enough to consider inviscid theory.) The inviscid equivalent of figure 5 is given in figure 7a, where the wall has been replaced by the image array of vortex elements. Naturally, the zero normal velocity at the wall implies a symmetric configuration only. The distance height 2h between the two arrays and the spacing between any two array elements are marked. This configuration will now be subject to three dimensional perturbations of the type exp ($i\alpha t$), having both spanwise and streamwise periodicities (as shown schematically in figures 7a and 7b). Again, symmetric perturbations are relevant because of the impermeability condition.

The required stability calculations have been made by Robinson & Saffman (1982). These calculations assume finite-core vortices, and show that the most unstable perturbations have a streamwise wavelength corresponding to the pairing mode, or the streamwise wavelength = $2\lambda_x$. Their results are given in figure 8, which is a plot of the normalized growth rate as a function of the spanwise wavelength λ_z/h. The parameter κ is $2h/\lambda_x$. Table 1 shows that κ is of the order 10^{-3} or lower for $R* > 100$.

Table 1

$R*$	$\kappa = 2h/\lambda_x$
10^2	5.10^{-3}
10^3	10^{-3}
10^4	3.10^{-4}

This means that the curve of interest to us here corresponds to $\kappa = 0$. It is worth pointing out that these calculations assume that the wavelength λ_z is large compared to the core size of the vortex elements. This will indeed turn out to be the case in the following. The results for $\kappa = 0$ and $\kappa = 0.2$ more or less overlap, and so even a few orders of magnitude variation in the estimates of λ_x (and hence κ) is immaterial for the results to be deduced from figure 8. This justifies our earlier assertion that the precise value of ν_e in (5) makes no difference.

Figure 8 shows that the growth rates are largest for two distinct spanwise wavelengths, say λ_{zs} and λ_{zl}; the two growth rates are comparable. This implies that the two-dimensional vortex structures get kinked on two distinct scales which, by virtue of their induced velocities, tend to form two distinct scales of Λ shaped eddies. It will be argued below that the smaller of the two corresponds to the so-called hairpin eddies (Head & Bandyopadhyay 1981), and the legs of the larger scale correspond to the so-called double roller structure.

The most amplified mode of the smaller of the two scales is given from figure 8 (after some slight rearrangement) to be

$$\lambda_{zs}\, U*/\nu = 1.7\, (U*\delta/\nu)^{0.5}. \qquad (6)$$

For the larger scale, the most amplified mode corresponds to

$$\lambda_{zl}/h = 17 \qquad (7)$$

In spatially developing flows, the observed wavelength is likely to correspond to the neutral mode (section 2); this changes (6) by only a few percent, while the estimate (7) gets altered from 17 to about 21.

We take the view that the presence in the TBL outer region of the hairpin-type structures is an established fact (Head & Bandyopadhyay 1981, Wallace 1984, Lynn

1987); however, there has been no serious effort made to obtain their wavelength quantitatively. From (6), it follows that $\lambda_{zs}U*/\nu$ varies between 55 at $R*$ of 10^3 and 170 at $R*$ of 10^4; this is consistent with the casual observation of Head & Bandyopadhyay (1981) suggesting a scale of the order 100 in roughly the same Reynolds number range. More work is obviously needed, but we tentatively conclude that the theory and experiment are in qualitative agreement.

For an experimental estimation of the larger wavelength, on which there is scant direct data, we have measured the correlation function $R_{uu}(\Delta z)$ between the velocity signals obtained from probes at a fixed height from the wall, separated by the variable distance Δz in the spanwise direction. The motivation is that, if there is some periodicity in the spanwise direction, a second peak must appear in the correlation function corresponding to the spanwise wavelength. Admittedly, these are not the optimum type of measurements to be made for this purpose, chiefly because of the degradation of the correlation by the superimposed small scale stuff, but it was believed that the spirit was consistent with the lack of sophistication at this stage of the rest of this work. A typical correlation function is given in inset to figure 9; in many instances, the second peak was substantially stronger. Even so, instead of directly basing the wavelength estimates on the position of the second peak, we chose for consistency to obtain them from the average of the first and second zero-crossings in the correlation function, which should correspond respectively to $\lambda_{zl}/4$ and $3\lambda_{zl}/4$. The results for two Reynolds numbers are plotted in figure 9. Also shown as two arrows marked (a) and (b) on the abscissa are the two values 17 and 21 for λ_{zl}/h. The data, lying generally between the two arrows, bear out the expectations from the theory.

Since λ_{zl} is large compared to h and, at moderate Reynolds numbers, is of the order δ itself, it seems reasonable to identify the legs of this Λ shaped structure with the double roller eddy deduced, among others, by Nagib & Guezennec (1986). Estimates from these latter measurements roughly confirm the present scaling.

One final remark may be useful. The existence of the log-law in the TBL suggests the possibility of a hierarchy of scales whose size varies with the height y from the wall. The inevitable randomization of the two scales discussed above will no doubt partly contribute to this, but one cannot rule out that other scales result from the interaction of these two primary ones.

6. The sublayer streaks

An ubiquitous aspect of the TBL structure in the inner layer concerns the sublayer streaks. Figure 10 shows the collection of all the data available on the spanwise spacing Λ of the streaks; $\Lambda^+ = \Lambda U*/\nu$. There is no discernible trend with Reynolds

number, and the mean spacing of around 100 wall units appears to be one of the solid quantitative results on which there is unusual agreement. So far as we are aware, however, there is no quantitative explanation for this remarkable observation. The interest in predicting this spacing is both fundamental and practical. For example, data in drag reduction by polymer addition or by stable stratification of the TBL show that there is a direct correlation between increased streak spacing and skin friction reduction.

The simplest possible explanation for these streaks is that they mark the tracks of the Λ-shaped eddies that are being dragged along. Unfortunately, neither of the two Λ structures discussed above has the observed constancy with Reynolds number (contrast equations (6) and (7) with figure 10), and so a different explanation appears called for. The one adopted in this section derives from the basic idea proposed by Coles (1978) and invoked in a similar context by Brown & Thomas (1977). The notion is essentially that when a 'big eddy' (which is two-dimensional on the streak spacing) moves with a convection velocity U_c, the particle paths under the eddy assume a curvature that is concave upwards (see figure 11a). The characteristic counterclockwise angular velocity ω is of the order $U_s/\mathbf{R}$, where U_s is the increased velocity at the sublayer edge, and $\mathbf{R}$ is the radius of curvature of the particle trajectory. It is reasonable to suppose that the velocity gradient in the sublayer (thickness δ_s) under the big eddy is increased, and the corresponding clockwise vorticity ζ is of the order U_s/δ_s. The connection to the Goertler instability is then clear, and the expectation that the observed streaks result from this mechanism is natural (see figure 11b).

For the notion to be useful, it is necessary to show (at least) that the following conditions hold. It should be shown by some kind of Floquet analysis that, among a host of other possible instabilities, it is indeed the Goertler instability that dominates. It should be shown that the two dimensional structures sketched in figure 11a are indeed present and are of sufficient strength. It should also be shown that the Goertler number Go exceeds the critical value substantially, and that the corresponding growth rates are large enough for the perturbations to grow to saturation amplitudes before encountering regions of convex curvature; these regions are expected to occur on either side of the concave region. The situation is hopeless in a strict sense, and all that we do here is to estimate the magnitudes of Go to render the notion somewhat plausible; we then estimate the streak spacing.

The obvious candidate for the two-dimensional 'big eddy' needed in this description is the two-dimensional roll-up structure that is presumed to exist before the onset of three dimensional instability. Although the growth rates of the three dimensional structures are large, leading to their eventual domination, there will be a certain part of the cycle over which the two dimensional structure can be expected to exist. Some

evidence for this can be found in short-time auto-correlation function of the u' velocity fluctuations; they reveal the character of lightly damped oscillators, with a distinct second peak occurring at some non-zero time lag, Δt^* (say). This second peak becomes insignificant if averaged for long periods of time, but is quite discernible when auto-correlations are obtained over durations of the order of a few hundred integral scales. The quantity Δt^* varies slightly from one short-time realization to another, and is distributed roughly like the Rayleigh distribution. Mean values of Δt^*, obtained for each Reynolds number from an ensemble of about thirty realizations, were converted to length scales using the convection velocity $U_c = 0.65\ U_\infty$. The data plotted in figure 12 show that $\lambda_x/\delta = O(6)$. We do not attach any significance to the fact that λ_x/δ increases slightly with Reynolds number, although there is no reason to rule out such a trend. The two curves shown in figure 12 correspond to the expression (5) for λ_x/δ, the difference between them being the choice for ν_e. The choices considered correspond to the Van Driest (1956) values at the location of either u'_{max} or q'_{max}. It is interesting that the data plot between the two curves. We shall argue presently that the approximate concurrence of λ_x/δ with the most popular bursting period is not mere accident.

In the present model, $U_c = 0.65\ U_\infty$, and we know h; the radius of curvature $\mathbf{R}$ will be bounded on the low end approximately by h itself. If the particle paths are assumed to be arcs of circle with chord lengths equal to the period $\lambda_x = 6\delta$, the upper bound for $\mathbf{R}$ can be estimated to be $6\delta\ (U*\delta/\nu)$. The upper bounds of Go, corresponding to the lower bound on $\mathbf{R}$, are of interest to us.

From the analysis by Floryan & Saric (1982) of the Gortler problem, it appears that we can write (in the notation of figure 11a)

$$U_s \Lambda/\nu\ (\Lambda/\mathbf{R})^{0.5} = \text{constant}$$

independent of the Goertler number. The precise value of the constant is a matter of some debate, but the one corresponding to the largest amplification rate is about 150 (figure 7 of Floryan & Saric's paper). Substituting h from (1) for $\mathbf{R}$, we have

$$U*\Lambda/\nu = (210/c)\ (U*\delta/\nu)^{1/6}$$

where $U_s = cU*$, c being a constant. If we assume a linear velocity distribution up to the edge of the sublayer, taken as usual to be 5 wall units in height, we obtain the result that

$$\Lambda U*/\nu = 42\ (U*\delta/\nu)^{1/6}. \qquad (8)$$

The main point is not the numerical constant on the right hand side, but the weak

dependence of the streak spacing on $R*$. The constant cannot be reliably estimated because there will be some acceleration of the sublayer right underneath the 'big eddy', and so c is possibly larger than 5; it needs only a 25% increase in the sublayer edge velocity for the above expression to yield the dashed line in figure 10. A simple plausible argument can be given to eliminate even the weak Reynolds number dependence in (8), but such detail is inconsistent with the spirit of this paper.

The precise values of the Goertler numbers attained are not easy to obtain, but rough estimates are possible. Recalling (in the present notation) that

$$Go = U_S\delta_S/\nu\,(\delta_S/\mathbf{R})^{0.5},$$

it is easy to show that Go decreases as $R*^{-0.25}$, but even at a fairly high value of 10^4 for $R*$, the estimated Goertler number is of the order 10. This value is above the critical values quoted for transition to turbulence. One may then be tempted to think of turbulent bursting as this transition to turbulence. It is obvious that Go is the largest right under the big eddies, and so, on the average, it is reasonable to expect this transition to occur at intervals comparable to λ_x. It will come as no surprise that many researchers have come up with the time interval between bursting to be of the order of $5\delta/U_\infty$.

7. Discussion and conclusions

Many instances have proven that flow control is better exercised when the dynamics are understood in terms of vortex interactions rather than, say, energy dynamics. This work arose from the awareness that there has been no such attempt made for the TBL as a unified whole. At this time, the principal merit of this work is probably the attempt itself, and its potential usefulnes lies in the clues that it might provide for control purposes. The model provides a self-generating mechanism for the TBL structure, and should therefore be capable of suggesting clues as to how one parameter, when influenced in a certain way, can alter the rest of the TBL characteristics. With this in mind, we have examined accelerated and decelerated boundary layers - including relaminarizing and separated cases - as well as the blade-manipulated boundary layers. A few interesting conclusions have emerged, but it seems better to use of the remaining space for emphasizing some of the inferences already alluded to in the text.

In summary, we have argued that the idealized version of the TBL is a vortex sheet located above the wall at a distance given by (1). Its primary instability yields the roll-up structures, which in turn excite the wall-layer streaks and bursting.The subsequent instability of the roll-up structures yields the hairpin eddies and the double roller structure.

The relative success of the linear stability analysis (here and elsewhere) in explaining the structural features of the highly nonlinear turbulent flows, can only be attributed to the fact that linearization is done 'cleverly'. Ordinarily, one linearizes about the 'experimental' mean velocity profile, without specifying how the profile was realized in the first place. This missing link is usually the 'ignorance factor'. Although the details of the mean velocity profile are unncessary in the present point of view, all ignorance is lumped in equation (1). For example, the configuration arrived at figure 7 is based on equation (1) and further logical consequences. This, however, represents the sole information required to proceed logically.

The second point is that the location of the peak Reynolds shear stress scales on the geometric mean of the inner and outer scales, more precisely according to (1). This implies that the most significant Reynolds stress producing activity does not occur at fixed y^+, and is in fact quite far removed from the wall region at high Reynolds number.

While $\overline{uv}$ does not scale on wall variables, the production of turbulent energy, $-\overline{uv}$ (dU/dy), does scale with y^+, at least roughly. Both the experimental data, and the data from fully developed pipe and channel flows obtained via (2), confirm that $-\overline{uv}$(dU/dy) peaks at y^+ in the vicinity of 15. (There may be some weak trend with $R*$, but this does not appear to be significant.) We conclude that the scales producing the Reynolds shear stress and the turbulence energy are quite distinct at sufficiently high Reynolds number. Perhaps the concept of 'active' and 'inactive' motion, hypothesized by Townsend (1961) and elaborated upon by Bradshaw (1967), has a bearing on the present picture.

If the above observation is taken to its logical conclusion, it appears to follow that bursting (as defined by the Stanford school in their seminal paper in 1967, and refined by them and others subsequently), which is an activity that occurs in the wall region ($y^+ < 30$, say), has to do mostly with energy production and not the Reynolds shear stress production. A further corollary is that if one is interested in the Reynolds shear stress, one should be measuring not at a fixed y^+ of 15 (or some such number) at all Reynolds numbers, but should follow the relationship given by (1). Such measurements are yet to be made in a systematic manner.

In the foregoing analysis, we have implied that the two dimensional and three dimensional structures coexist in general, the two dimensional configuration being only the intermediate state. Since the three dimensional instabilities are the faster growing ones, it is the three dimensional structures that we typically find, and the strength of the two-dimensional motion in a long-time average is quite weak. Indirect estimates confirm this. The structure of the TBL is thus largely three dimensional (the

picture being surprizingly close to that of Theodorsen 1955), and it follows that all successful 'active' control schemes must also be three dimensional. From the measurements of Nagib & Guezennec, it appears that the strength of the double roller structure is weak also, but all indications are that the smaller scale hairpin type eddies are quite strong and represent the truly coherent motion in the main part of the TBL. It appears that successful outer layer management of the TBL must concentrate on these structures. We believe that one (though not necessarily the most important) function of the blade manipulators is to act on these hairpin eddies (Lynn 1987). A more detailed discussion will be given elsewhere.

Since we did not have to make special distinction between channel (and pipe?) flows and TBLs in terms of the structural features, we speculate that they are essentially similar over a major part of the flow except where the two sides start to interact together in the channel flow.

Finally, as mentioned towards the end of section 6, the present theory suggests that the Goertler number decreases with $R*$ as its -1/4 power. The implication is that at very high $R*$, the Goertler number does not become large enough for streak formation. Whether this is really the case is not known, and it is possible that roughness effects will render this an academic question.

Acknowledgements

I am grateful to Anatol Roshko and Mark Morkovin for acting as effective sounding boards on two important occasions. I have benefitted from discussions with a number of colleagues, and learnt especially from questions raised by Steve Kline, Roddam Narasimha and Kirit Yajnik; if they have not been answered satisfactorily, it should be said that it is not for lack of effort. My thanks go to Ted Lynn who provided me the data of figure 9, to Charles Meneveau, S Raghu and R. Ramshankar for commenting on the manuscript, and Jim McMichael for his initial enthusiasm for the work as well as for the AFOSR support.

Appendix

Other indirect evidence can be given to support the notion that the maximum stress region in the TBL is like a critical layer. The skewness of u' (for example) is negative close to the wall, and is positive in the outer region. Its value is close to zero in a part of the overlap region including the 'critical layer'. More significantly, in the part below the peak stress region, the so-called high-frequency pulses (that is, signals which are narrow-band-pass filtered around a fairly high center frequency) tend to occur during the positive half of the unfiltered signal while doing the reverse in the part above that region (Badri Narayanan, Rajagopalan & Narasimha 1977). These

observations, taken together, can be interpreted to mean the presence of something like a phase jump across the 'critical layer'. Naturally, the concept of phase jump for random signal is ill-defined, but loose arguments can be given in support of the present notion.

References

Achia, B.V. & Thompson, D.W. 1976 J. Fluid Mech. 81, 439.
Andreopoulos,T., Durst, F., Zaric, Z. & Jovanic, J. 1984 Exp. in Fluids 2, 7.
Badri Narayanan, M.A., Rajagopalan, S. & Narasimha, R. 1977 J. Fluid Mech. 80, 237.
Blackwelder, R.F. 1978 In Lehigh Workshop on Coherent Structure in Turbulent Boundary Layers, ed. C.R. Smith & D.E. Abbot, p 211.
Blackwelder, R.F. & Kaplan, R.E. 1976 J. Fluid Mech. 107, 89.
Bradshaw, P. 1967 J. Fluid Mech. 30, 241.
Bremhorst, K. & Walker, T.B. J. Fluid Mech. 61, 173.
Brown, G.L. & Thomas, A. W. 1977 Phys. Fluids 20, s243.
Cantwell, B.J. & Coles, D.E. 1983 J. Fluid Mech. 136, 321.
Coles, D.E. 1978 In Lehigh Workshop on Coherent Structure in Turbulent Boundary Layers, ed. C.R. Smith & D.E. Abbot, p 462.
Falco, R.E. 1977 Phys. Fluids 20, s124.
Falco, R.E. 1987 Presentation at the Workshop on Turbulent Boundary Layer, Austin,Texas.
Floryan, J.M. & Saric, W.S. 1982 A.I.A.A. 20, 316.
Gaster, M., Kit, E. & Wygnanski, I. 1985 J. Fluid Mech. 150, 23.
Gupta, A.K & Kaplan, R.E. 1972 Phys. Fluids 15, 981.
Gupta, A.K., Laufer, J. & Kaplan, R.E. 1971 J. Fluid Mech. 50, 493.
Head, M.R. & Bandyopadhyay, P. 1981 J. Fluid Mech. 107, 297.
Hussain, A.K.M.F. 1981 Proc. Ind. Acad. Science (Engg. Science) 4, 129.
Johansson, A.V. & Alfredsson, P.H. 1982 J. Fluid Mech. 122, 295.
Jordinson, R. 1970 J. Fluid Mech. 43, 801.
Kim, J. & Moin, P. 1986 J. Fluid Mech. 162, 339.
Kim, H.T., Kline, S.J. & Reynolds, W.C. 1971 J. Fluid Mech. 50,133.
Klebanoff, P.S. 1954 NACA Rep. 1247.
Kline, S.J., Reynolds, W.C., Schraub, F.A. & Runstadler, P.W. 1967 J. Fluid Mech. 30, 741.
Kline, S.J. 1978 In Lehigh Workshop on Coherent Structure in Turbulent Boundary Layers, ed. C.R. Smith & D.E. Abbot, p 1.
Kudva, A.K. & Sesonske, A. 1972 Int. J. Heat Mass Tr. 15, 127.
Kovasznay, L.S.G., Kibens, V. & Blackwelder, R.F. 1970 J. Fluid Mech. 41, 283.
Laufer, J. 1951 NACA Rep. 1053.
Laufer, J. 1954 NACA Rep. 1174.

Lee, M.K., Eckelman, L.D. & Hanratty, T.J. 1974 J. Fluid Mech. 66, 17.
Lynn, T.B. 1987 Ph. D. Thesis, Yale Univ..
Monin, A.S. & Yaglom, A.M. 1971 Statistical Fluid Mech. vol. I, M.I.T. Press.
Nagib, H.M. & Guezennec, Y.G. 1986 Paper prepared for Proc. Symp. on Turbulence, Univ. Missouri-Rolla.
Nakagawa, H. & Nezu, I 1981 J. Fluid Mech. 104, 1.
Nikuradse, J. 1932 Forsch. Arbeiten Ing.- Wesen, no. 356.
Oldaker, D.K. & Tiederman, W.G. 1977 Phys. Fluids. 20, s133.
Perry, A.E. & Chong, M.S. 1982 J. Fluid Mech. 119, 173.
Praturi, A.K. & Brodkey, R.S. 1978 J. Fluid Mech. 89, 251.
Ramshankar, R. 1986 Yale Univ. Rep 86FM5.
Rao, K.N., Narasimha, R. & Badri Narayanan, M.A. 1971 J. Fluid Mech. 48, 339.
Reynolds, W.C. & Tiederman, W.G. 1967 J. Fluid Mech. 27, 253.
Robinson, A.C. & Saffman, P.G. 1982 J. Fluid Mech. 125, 411.
Schildknecht, M., Miller, J.A. & Meir, G.E.A. 1979 J. Fluid Mech. 90, 67.
Schraub, F.A. & Kline, S.J. 1965 Stanford Univ. Rep no. MD-12.
Smith, C.R. & Metzler, S.P. 1983 J. Fluid Mech. 129, 27.
Sreenivasan, K.R., Tavoularis, S. & Corrsin, S. 1982 In Turb. Shear Flows III, ed. Bradbury et al. p.96., Springer-Verlag.
Theodorsen, T. 1955 In 50 Jahre Grenzschichtforschung, ed. Goertler & Tollmien, Vieweg & Sohn
Thorpe, S.A. 1971 J. Fluid Mech. 46, 299.
Thorpe, S.A. 1973 J. Fluid Mech. 61, 731.
Townsend, A.A. 1956 The Structure of Turbulent Shear Flow, Cambridge University Press.
Townsend, A.A. 1966 J. Fluid Mech. 26,689.
Ueda, H. & Mizushina, T. 1977 In Proc. 5th Biennial Symp. on Turb. Univ. Missouri-Rolla.
Van Driest, E.R. 1956 J. Aero. Sci. 23, 1007.
Willmarth, W.W. & Bogar, T.J. 1977 Phys. Fluids 20, s9.
Wygnanski, I. 1987 This Proceedings.
Wygnanski, I., Champagne, F.H. & Marasli, B. 1986 J. Fluid Mech. 168, 31.

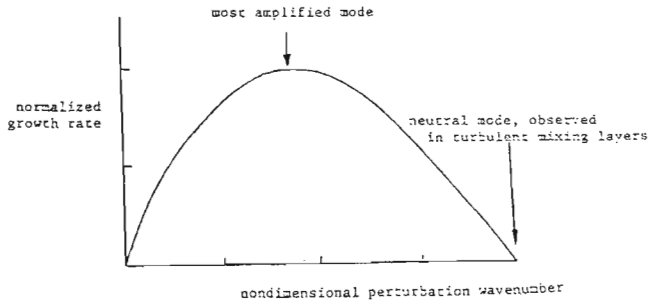

Figure 1. Schematic of the normalized amplification rates for a finite thickness vortex sheet

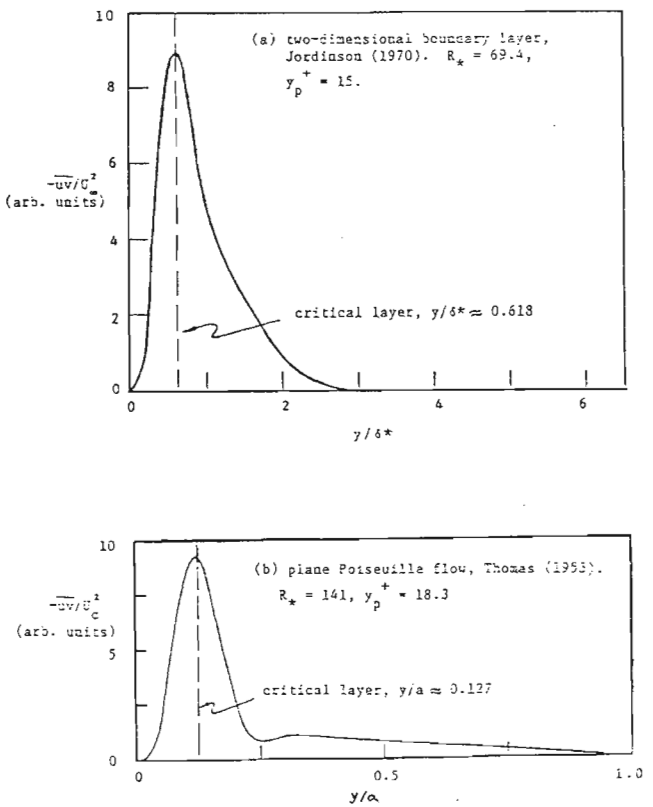

Figure 2: The distribution of the Reynolds shear stress in (a) boundary layer and (b) channel (plane Poiseuille) flows, evaluated from the numerically computed eigensolutions. The eigensolution data in (a) were from Jordinson (1970), and in (b) from Thomas (1953). These latter calculations were made by Stuart: see, for example, Drazin & Reid's book.

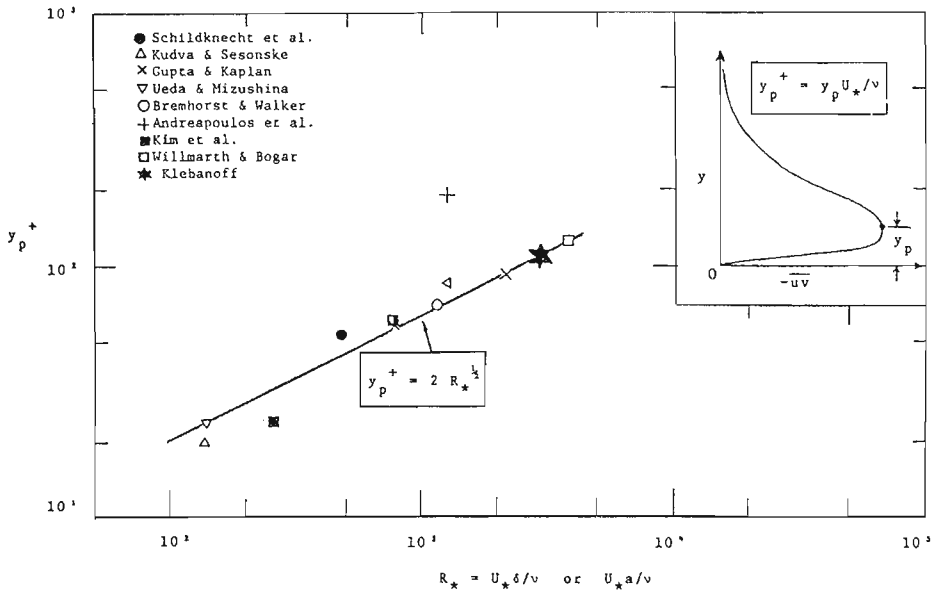

Figure 3a: The peak Reynolds shear stress location in boundary layers, pipe flows and channel flows. Data from various measured Reynolds stress distributions.

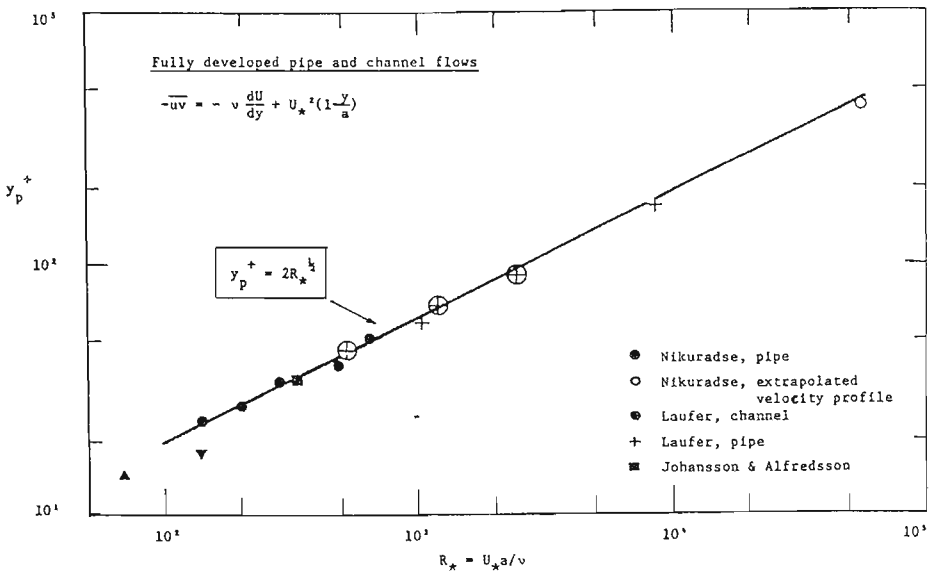

Figure 3b: The peak Reynolds shear stress location in fully developed pipe and channel flows, computed from the measured mean velocity distributions.

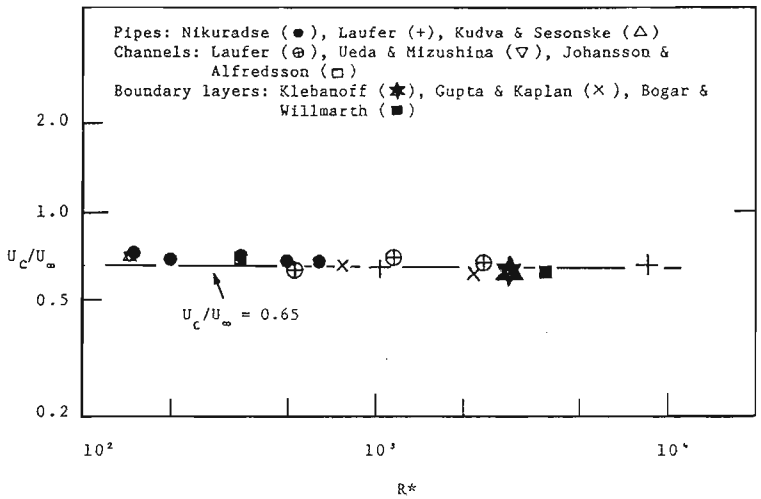

Figure 4: The mean velocity at the peak Reynolds shear stress location in boundary layers, channel and pipe flows.

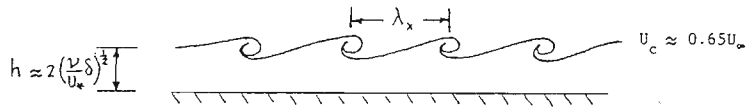

Figure 5. The roll-up of the vortex sheet placed at the 'critical layer'

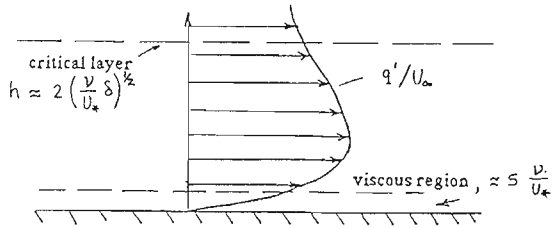

Figure 6. The 'critical layer', and the distribution of the turbulence intensity

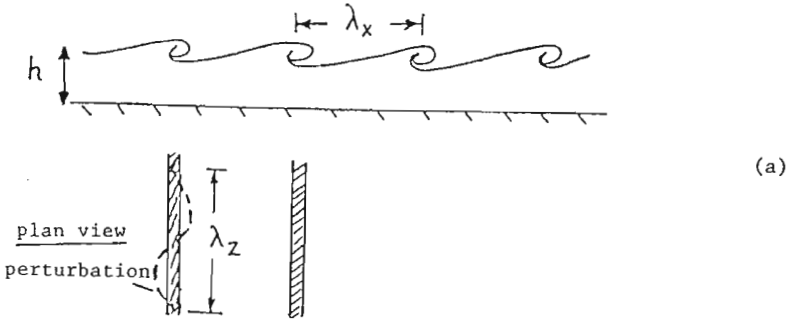

Inviscid version

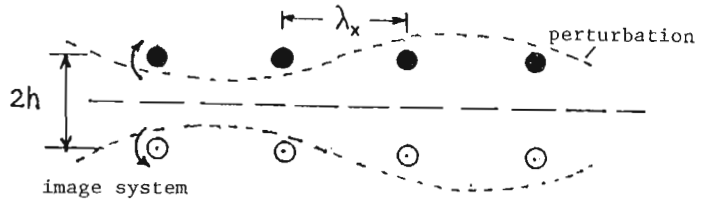

streamwise wavelength arbitrary

Figure 7

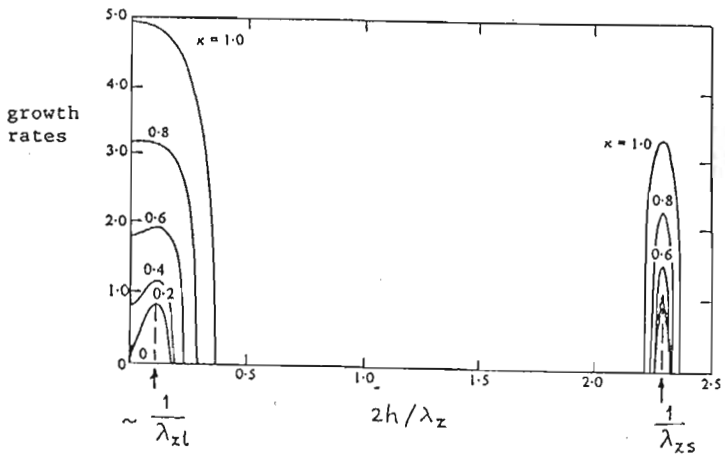

Figure 8. Amplification rates from the three-dimensional stability calculations for the inviscid version in figure 7. This figure is here reproduced from Robinson & Saffman (1982)

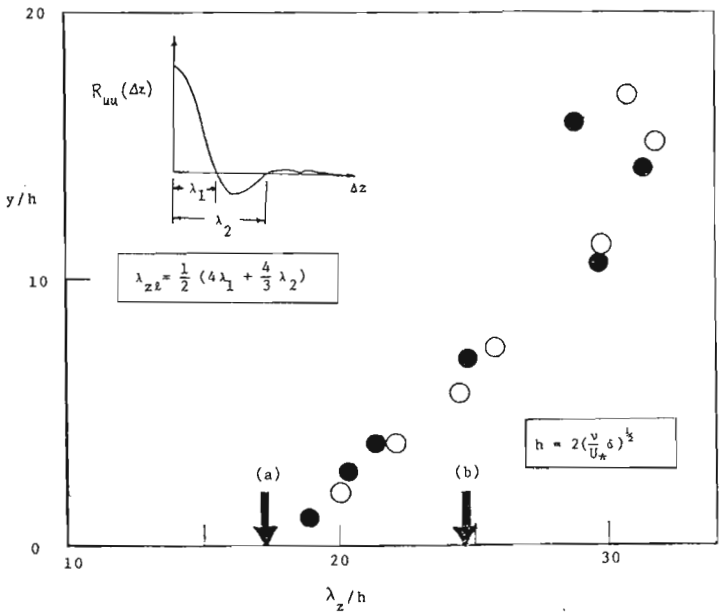

Figure 9: A measure of spanwise scale developed due to the three-dimensional instability in the present vortex model. This curve is based on measurements in turbulent boundary layers by T.B. Lynn. ●, U_* = 77.9 cm/sec, δ = 2.43cm; ○, U_* = 75.8 cm/sec, δ = 2.85 cm. The arrow at (a) corresponds to the most amplified wavelength, as deduced here from the calculations of Robinson & Saffman (1982); that at (b) corresponds to the neutral wavelength.

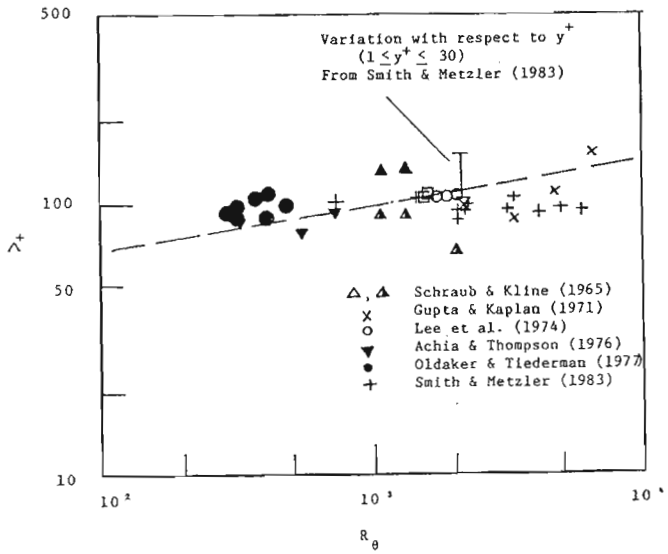

Figure 10: The spanwise streak spacing Λ^+, normalized by viscous units. All measurements have been made below a y^+ of about 30. Techniques of measurement differ from one source to another.

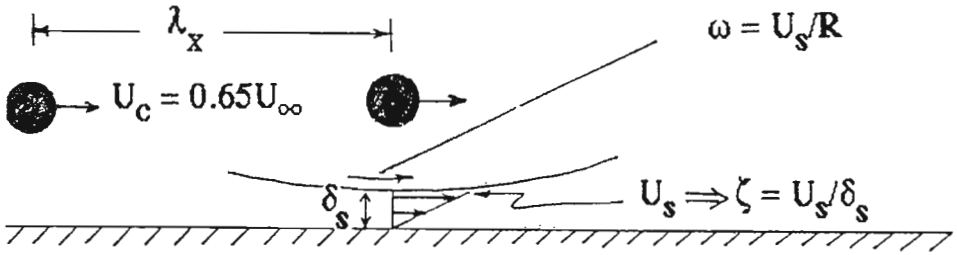

Figure 11a

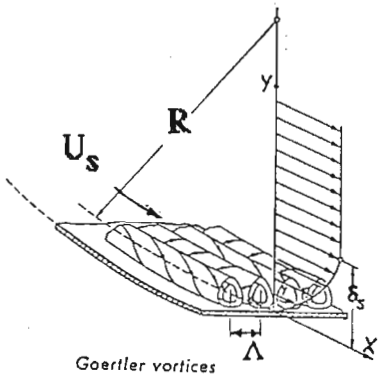

Figure 11b

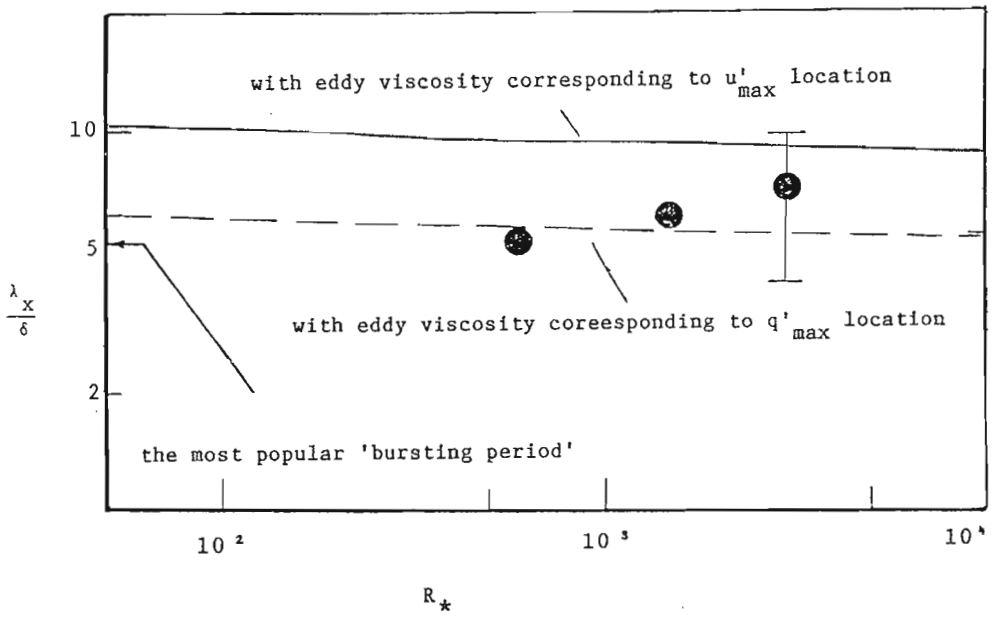

Figure 12: The second peak in the short-time auto-correlation function measured in the peak stress region, averaged approximately over 30 realizations. The time scale is converted to the spatial scale using the convection velocity at the peak stress region (the 'critical layer'). The interpretation is that this quantity represents the streamwise wavelength of the primary inviscid instability of the present vortex sheet model. The full and dashed lines are estimates based on vorticity diffusion and convection arguments discussed in the text. For the full line, vorticity is assumed to be diffused by eddy viscosity appropriate to the peak u' location; the dashed line, representing similar calculations with eddy viscosity of the peak q' location ($q'^2 = \overline{u'^2} + \overline{v'^2} + \overline{w'^2}$) is perhaps more representative, but is unfortunately less certain in terms of the numerical accuracy because of the paucity of data on q' over a wide range of Reynolds number.